

# A Soft, Modular, and Bi-stable Dome Actuator for Programmable Multi-Modal Locomotion

Michael A. Bell<sup>\*1</sup>, Luca Cattani<sup>\*2</sup>, Benjamin Gorissen<sup>1</sup>,  
 Katia Bertoldi<sup>1</sup>, James C. Weaver<sup>1</sup>, and Robert J. Wood<sup>1</sup>

Abstract— Movement in bio-inspired robots typically relies on the use of a series of actuators and transmissions with one or more degrees of freedom (DOF), allowing asymmetrical ellipsoidal gaits for use in walking, running, swimming, and crawling. In an effort to simplify these multi-component systems, we present a novel, modular, soft, bi-stable, one DOF dome actuator platform that is capable of complex gaits through mechanical programming, driven by simple periodic fluid input. With a modular, reconfigurable design, the end effectors of these bi-stable dome actuators can be quickly modified for use on a variety of surfaces for specific applications. In the present study, we describe the finite element modeling, manufacturing, and characterization of different end effectors and outline a workflow for the implementation of these soft bi-stable dome actuators for the production of functional robotic prototypes.

## I. INTRODUCTION

Motivated by the need to develop robots that possess the capabilities to traverse a wide range of complex topographies, many engineers have turned to nature for design inspiration. As a result, a diverse array of legged robots have been created, equipped with an equally diverse array of actuators to achieve animal-like gaits. These robots span multiple length scales and incorporate a wide range of force generation systems, ranging from the use of piezoelectric actuators in cockroach-scale robots [1], to custom electromagnetic motors in large cheetah-like designs [2]. Unfortunately, additional degrees of freedom in robotic appendages or the controlled switching between different gaits for terrain-specific mobility typically comes with added complexity in terms of both the mechanical design of the appendages and their associated control systems [3], [4]. In an effort to develop more robust and cost-effective robotic prototypes, soft pneumatic or hydraulic actuators have recently attracted a great deal of attention [5], [6], [7], [8]. Soft actuators offer many advantages over their more traditional rigid counterparts, ranging from increased robustness and damage tolerance to ease of fabrication [9], [10], [11], [12]. Despite these advantages, the creation of efficient

gaits in soft robotics is challenging [13], or requires the use of large numbers of bellow-like actuators [14], [15], with equally complex control systems [16].

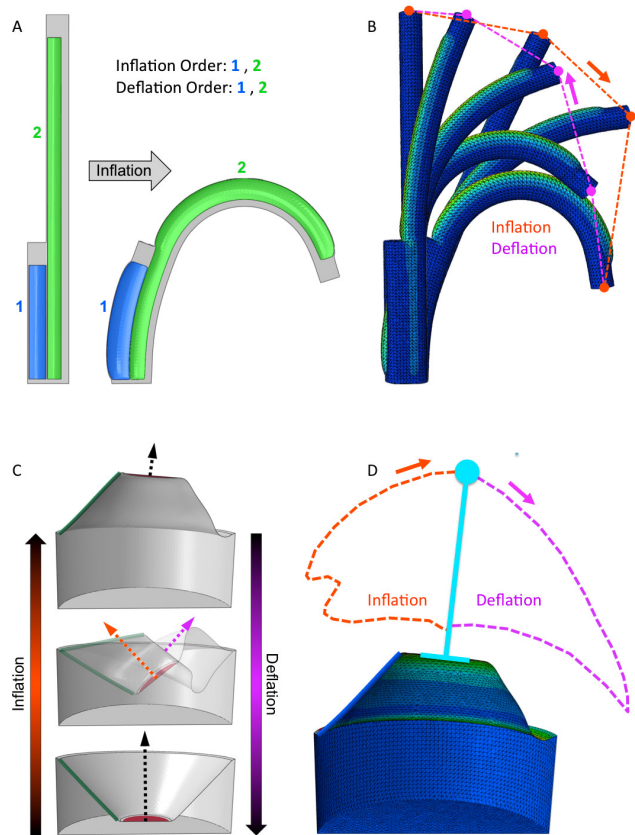


Fig. 1. (A-B) A cilia-like linear actuator which requires two chambers to achieve an asymmetric gait cycle, compared to our newly developed bi-stable dome actuator (C-D), demonstrating that a single inflation/deflation cycle can produce an asymmetric gait, reducing the DOFs to one. [17]

An alternative soft actuator design that circumvents many of these limitations is a path-dependent nonlinear domed actuator, which can be mechanically programmed through the incorporation of asymmetrical rib-like elements into the dome structure [18]. The different features of these actuators (dome angle, wall thickness, rib location, etc.) can in turn be leveraged to create a useful gait, thus reducing the complexity of the associated power and control systems. While traditional legged robots typically require one or more actuators, such as motors or pistons, and transmission components such as gears, shafts, and

<sup>\*</sup>Michael A. Bell and Luca Cattani are co-first authors. This work was supported by the Office of Naval Research (award # N00014-17-1-2063) and the Wyss Institute for Biologically Inspired Engineering.

<sup>1</sup>John A. Paulson School of Engineering and Applied Sciences and the Wyss Institute for Biologically Inspired Engineering, Harvard University, 60 Oxford Street, Cambridge, MA 02138, USA.

<sup>2</sup>Swiss Federal Institute of Technology Lausanne (EPFL), Switzerland.

bell@seas.harvard.edu luca.cattani@alumni.epfl.ch

bearings, dome actuators merely require pulsing of fluid against a monolithic soft membrane to create a gait cycle, which can be highly efficient and repeatable systems [19]. These actuators can be driven with a wide range of fluids, pneumatically or hydraulically, depending on the surrounding medium such as seawater or air. Notably, compared to traditional bellow-type soft actuators [17], dome actuators can effectively reduce the DOFs required to create a simple asymmetrical sweeping motion (Figure 1).

Previously, we fabricated a simple, tethered "PlanarBot" capable of harnessing nonlinear actuator gaits to move in a programmed direction [18]. The dome actuators developed at that time, however, were limited in their payload, and the retraction and actuation paths were highly influenced by contact forces when the robot was loaded. The developments reported in the present study have largely mitigated those previous design and performance limitations, while focusing on end-effector design, manufacturing, and characterization.

## II. Bistable Dome

Our updated dome actuator consists of a truncated cone with slant angle  $\alpha$ , outer radius  $R$ , and a radial rib-like thickening with a circular cross-section (see Figure 1 (c), where the thickened rib is colored in green). To simulate the response of our actuators upon inflation and deflation, we conducted Finite Element (FE) analyses within the commercially-available software ABAQUS (Dassault Systèmes). The models were constructed using shell elements (Abaqus element code: S4R) and the rib-like thickening was modeled by introducing a line of beam elements (Abaqus element code: B31) running along the slanted edge of the cone. The response of the rubber was captured using an incompressible neo-Hookean model, with an initial shear modulus,  $\mu = 0.14$  MPa. The structure was loaded by supplying incompressible fluid to the internal cavity in a dynamic implicit loading step, and a small amount of damping (stiffness proportional Rayleigh damping,  $\beta = 0.01$ ) was introduced to account for all dissipative processes.

In a first analysis, we considered an actuator with  $\alpha = 10^\circ$ , for which we report the normalized Pressure-Volume (PV) relationship and corresponding deformations in Figure 2A. From these analyses, we discovered that the PV-curve was monotonic in volume, and as an unsurprising consequence, the actuator displayed the same deformation during inflation and deflation, thus exhibiting no enclosed area within a single inflation-deflation cycle. This behaviour is clearly seen in Figure 2A, where the arrow indicates the normal on the cone's apical surface, which points in the same direction during inflation and deflation. However, for larger slant angles ( $\alpha > 15^\circ$ ), the actuator behaved fundamentally different. This is evident in Figure 2B, where we present results for a performance-optimized actuator with  $\alpha = 47.5^\circ$ . For this actuator (whose detailed multi-component struc-

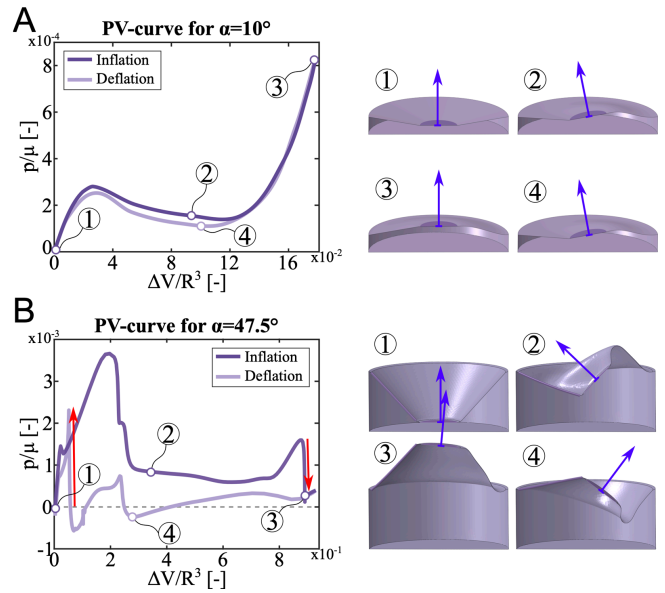


Fig. 2. Finite Element Analysis of two actuator designs with slant angles  $\alpha$  of  $10^\circ$  (A) and  $47.5^\circ$  (B). The left figures show the simulated pressure-volume relationships, with corresponding deformations shown on the right.

tural optimization workflow will be presented elsewhere), inflation and deflation followed a different path that was characterized by highly dynamic snapping events as shown in Figure 2B (red arrows). The enclosed area that we see on the PV-diagram is thus not an effect of material hysteresis, but originates from the mechanics of the structure. An analogous form of path asymmetry has been reported for shallow arches, where limit points in displacement lead to enclosed areas in the force-displacement curves [20]. In contrast to spherical domes [21], where due to axisymmetry, the deformations do not show an enclosed area, we were able to harness the enclosed area in PV by adding a radial rib-like feature that broke the deformation symmetry. The resulting deformations were completely different between inflation and deflation, as shown in Figure 2B, where the normal on the apex points are in different directions during loading (2) and unloading (4).

To experimentally validate our FE analyses, we molded the actuator with a slant angle of  $47.5^\circ$  out of Smooth-Sil 945 (Smooth-on, Macungie, PA, USA), and during one loading cycle, we tracked the displacement of a circular marker that was rigidly connected to its apex plate. The asymmetrical displacement curves obtained from these experiments showed qualitative agreement with our FE analyses, as shown in Figure 3, demonstrating their potential usefulness in effectively creating gait-like circular motions.

## III. Bi-stable Dome Manufacturing and Tip Geometry

### A. Manufacturing Process

To create thin, complex, and small-scale features, the use of traditional soft robotic molding approaches,

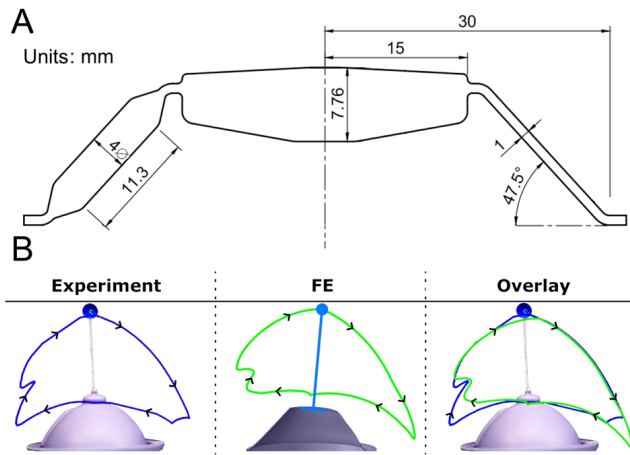


Fig. 3. (A) Dimensions of the the molded base, for the soft, modular bi-stable dome actuator. (B) Left: Experimental results obtained from end tracking of our domed actuator. Middle: FE simulation of the same geometry using measured material parameters. Right: Strong agreement between experimental tracking and FE simulation. The small discrepancies in the data at the bottom left and right regions of the path trajectory plots are due to physical interactions between the thin cylindrical pin (which was not present in the simulation, and connects the dome to the tracking ball) and the side wall of the domed actuator.

consisting of pouring silicone into two open faced molds, followed by subsequent mating of the two halves [7], was not a viable strategy. Generally, silicone viscosity increases with durometer, and so in order to obtain higher forces from the dome, a higher durometer silicone was used (45A Shore Hardness). To resolve the small features required for its successful operation, liquid silicone injection molding was used, which allowed for high enough injection pressures to reach all of the fine features within the mold. In addition, more complex shapes and features could be obtained through this approach, such as thin overhang features, or the incorporation of embedded components. The injection mold was 3D printed using an Objet30 inkjet-based 3D printer (Stratasys, Eden Prairie, MN, USA) from VeroClear (RGD810) material. The molds were designed with appropriate gates, runners, and vents for material evacuation during the injection molding process. A custom injection molding station was employed for this purpose, which consisted of an Albion AT1500X air-powered cartridge gun (Albion Engineering, Moorestown, New Jersey, USA) and a Nordson EFD Series 480 Optimixer (part #7361707, East Providence, RI, USA) static mixing nozzle, using a 1:1 part silicone (Smooth-Sil 945 Smooth-On, Macungie, PA).

The mold (Figure 4), contains three upper cores and one lower core. The upper cores allow for the successful removal of the complex overhanging shape. The mold vents were placed exactly 180° apart to allow air to evacuate the mold as injected silicone circumvented the dome geometry. All cores were bolted together using M5 bolts and square insert nuts and torqued down to provide a tight seal on all parting surfaces to minimize

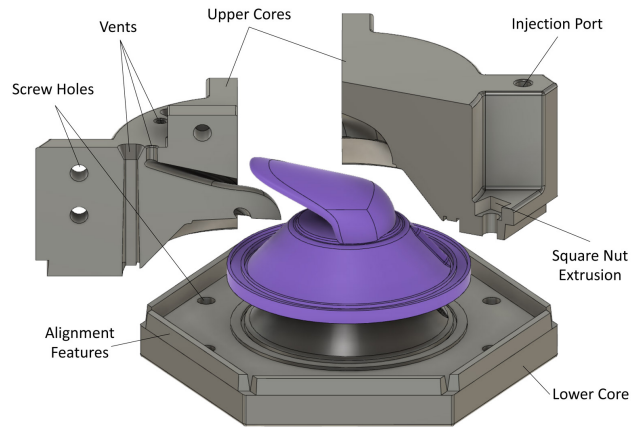


Fig. 4. Injection mold design creating the integrated "duckbill" shape, which contains a complex overhang requiring three upper cores for successful demolding. The third upper core, which is a mirror of the upper left core is hidden, for clarity purposes.

flashing. Liquid silicone was injected at up to 827 kPa (120 psi) until material flowed out of all vents for at least 30 seconds. The mold was then placed in an oven at 65°C for 30 minutes to complete the curing process. All fasteners were then removed, followed by the lower core and then the upper cores. Excess cured material left in the gate and vent holes were then manually trimmed.

#### B. Modular and Integrated End Effectors

To harness gait motions of the bi-stable domes in various environments, different end effectors were designed to maximize locomotion speed over various conditions/substrates. Instead of creating a separate injection mold for all possible iterations of the end effectors, a modular platform was designed to allow rapid prototyping of end effectors as shown in Figure 5. The modular assembly consisted of a bi-stable dome, with a custom laser-cut stainless steel insert washer and a press-fit M3 nut, fully embedded within the dome top. Multiple iterations of end effectors could then be quickly and easily swapped with a simple change of a screw. Saw-tooth features were designed into the mating end effector to prevent rotation of these modular tips as they were screwed down into the embedded nut. Each end effector was 3D printed out of carbon fiber-reinforced nylon on an Onyx One 3D printer (Markforged, Somerville, MA, USA), or from the "Tough" photo-polymer on a Form3 3D printer (Formlabs, Somerville, MA, USA), for all of our tests.

Once an end effector was chosen and sufficiently evaluated, an injection mold could then be constructed with that specific tip geometry to create a fully integrated dome - end effector construct. Figure 6 shows a duckbill-like end effector with a modular 3D-printed rigid tip (A) and its fully integrated soft-molded counterpart (B). During this design process, differences in the material properties between the 3D-printed rigid end effector and the dome elastomer had to be taken into consideration

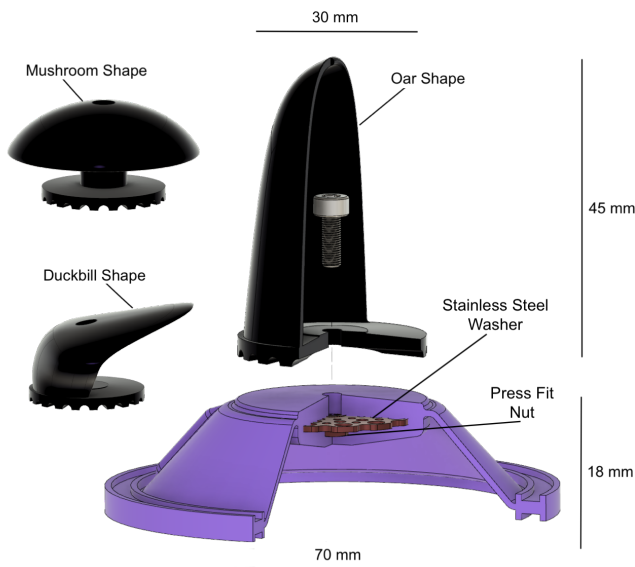


Fig. 5. Modular dome assembly cross section, with a selection of morphologically distinct end effectors. A custom laser-cut stainless steel washer with embedded nut allowed for quick and easy swapping of end effector tips for evaluation on different terrains.

when designing the geometry of the fully integrated injection-molded geometry in order to achieve similar behaviours.

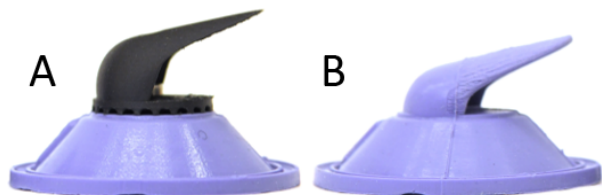


Fig. 6. Modular rigid 3D-printed duckbill-shaped end effector (A), and its integrated injection-molded single-material counterpart (B) attached to identical dome geometries.

### C. Environments

While there are a myriad of potential environments on which to test the dome actuators, three different environments were chosen for initial testing and characterization; a rigid surface (vinyl flooring), a compliant granular medium (sandbox sand), and water.

To demonstrate the dome actuator gait, different end effectors, each specifically tailored for a specific environment [22], were designed, 3D printed, and evaluated (Figure 5). For walking on a hard surface, a single contact point was used to maximize displacement per gait cycle [23], [24]. To permit operation on a granular medium, the tip was expanded into a spherical dome or mushroom-like shape to distribute the force over a larger area [25], [26].

For swimming in water, a large perpendicular surface area normal to the direction of motion is most efficient. Oar-like tips with a convex shape to maximize the power

stroke and minimize the recovery stroke's drag were thus designed, and elongated to maximize the area [27], [28].

Lastly, a hybrid between the mushroom and oar shape was designed to function in all three environments. This duckbill-like design has a convex shape to maximize the power stroke, while having a curved top surface for use on rigid surfaces. The large curved surface also increased the surface area for load distribution on sand.

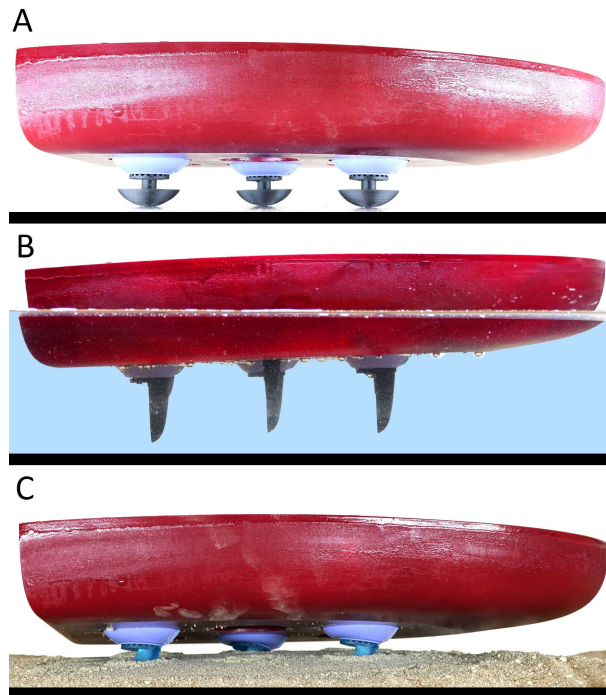


Fig. 7. The amphibious robotic prototype moving on three different surfaces: (A) mushroom-shaped end effectors walking on a hard vinyl surface, (B) oar-shaped end effectors for swimming in water, and (C) duckbill-shaped end effectors for walking on sand.

## IV. Robot Demonstrator

To effectively demonstrate the multi-modal usage of the developed soft bi-stable dome actuators, a platform in the shape of a simple boat hull was designed to hold a 2x3 array of actuators. The boat, 42 cm x 30 cm x 6.5 cm, 2.4 kg, allowed for all on-board pumps, valves, batteries, and electronics to power the robot for untethered operation.

### A. Design, Control, and Actuator Integration

The dome actuators achieved a full gait cycle by inflating to ca. 15 kPa and deflating to ca. -15 kPa through the use of two Parker Hannifin BTC-IIS Miniature Diaphragm Pumps operating in parallel (Parker Hannifin Corporation, Cleveland, OH, USA) in a closed pneumatic system. Upon initialization, channel A's domes were in the actuated state and over-pressurized to ca. 20 kPa by a fill port, while channel B had all of its air removed by collapsing the soft dome actuators by hand. Once initialized, the pneumatic system operated by pumping air from the high pressure side to the low pressure side,

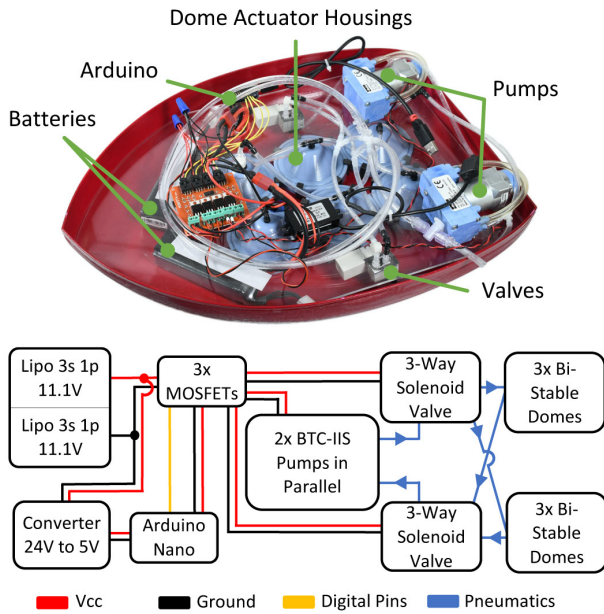


Fig. 8. Photograph of the amphibious robot used to demonstrate the utility of the dome actuators (upper), and its schematic (lower).

with the two channels acting  $180^\circ$  out of phase to achieve forward movement. The two identical pumps were used in parallel to increase the flow rate, and therefore increase the cycle rate.

The soft dome actuators were designed with an elastomeric seal that was clamped between the boat hull and a rigid mounting flange. The dome mounting flange was clipped into place at multiple points to allow easy installation and removal as the optimization of the dome actuators evolved. The dome flange was designed to minimize dead volume such that a higher pumping efficiency could be achieved, and ultimately a faster cycle rate. All electronics and pneumatics were attached to a laser cut removable tray for easy servicing, charging of the batteries, or updating of the microcontroller code.

The electrical and pneumatics system diagrams are shown in Figure 8. The entire system runs on 24 V using two 3S 2200 mAh LiPo batteries operating in series. A 24 V to 5 V DC switching power supply was used to power the Arduino and MOSFET board. The pumps and two valves were controlled through the MOSFET board by digital outputs from the Arduino. Two solenoid valves, Clippard 15 mm series 3-Way NC valves (E315F-2L024, Clippard, Cincinnati, OH), allowed the flow direction to be switched between the two channels.

A 2x3 actuator array was chosen to allow for three points of stability during extending and retracting modalities (i.e., for alternating tripod gaits), and the channel configuration is shown in Figure 8. As each channel is  $180^\circ$  out of phase, one channel begins to extend while the other channel retracts. This configuration reduced the time between two steps, as the volume to inflate was smaller and there was no distinct step-

TABLE I

Cost of transport for different end effectors and environments.

	Hard Surface	Sand	Water
Mushroom	404	3214	503
Oar	*	*	46.4
Duckbill	725	1127	85.7

Examples denoted with an asterisk did not make forward progress.

recovery phase, compared to cases where all of the soft dome actuators were inflated and deflated together.

## V. Characterization and Gaits

The robot achieved a 0.167 Hz cycle rate, using two offset channels, with their corresponding operating pressures shown in Figure 10.

The robot's performance in the three different environments with the three end effectors were compared using the dimensionless unit, cost of transport (COT), to better compare the whole system performance. These results also demonstrate that the reduction of the whole system's power and weight can lead to great improvements in COT in future design iterations. The amphibious robot achieved a maximum walking rate of 1.18 mm/s (COT of 404) on the hard Vinyl terrain with the mushroom-shaped end effector, a swimming rate (in water) of 10.3 mm/s (COT of 46.4) with the oar-like end effector, and a speed of 0.42 mm/s (COT of 1127) with the duckbill-shaped end effector on sand. As expected, the rolling contact point made it easier to advance on hard surfaces, but didn't help much on granular terrains. In contrast, the hybrid duckbill-shaped end effector was more efficient on sand due to its more aggressive angle of attack, generating a greater normal force in the direction of motion, and achieved a balance of performance between those observed between the oar-shaped and mushroom-shaped designs.

## VI. CONCLUSIONS AND FUTURE DIRECTIONS

In the present study, we developed a soft, bi-stable, modular, path-dependent, single-input actuator that could be leveraged to perform effective asymmetrical gait-like actuation cycles. Our design process and experimental results demonstrate the intrinsic versatility of these dome actuators that can be achieved through simple modifications to the end effector geometry. Through the incorporation of these actuators into an experimental test bed, we were able to produce an amphibious robot that was able to walk on both hard and sandy surfaces as well as propel itself through water with a single end effector design. There is much that remains to be explored in this exciting new design space of domed actuators. For example, the implementation of a generative design workflow could be used for further optimization of the dome parameters and end effector geometry for more robust walking and swimming. Custom gaits, potentially by prescribing the desired gait and working backwards

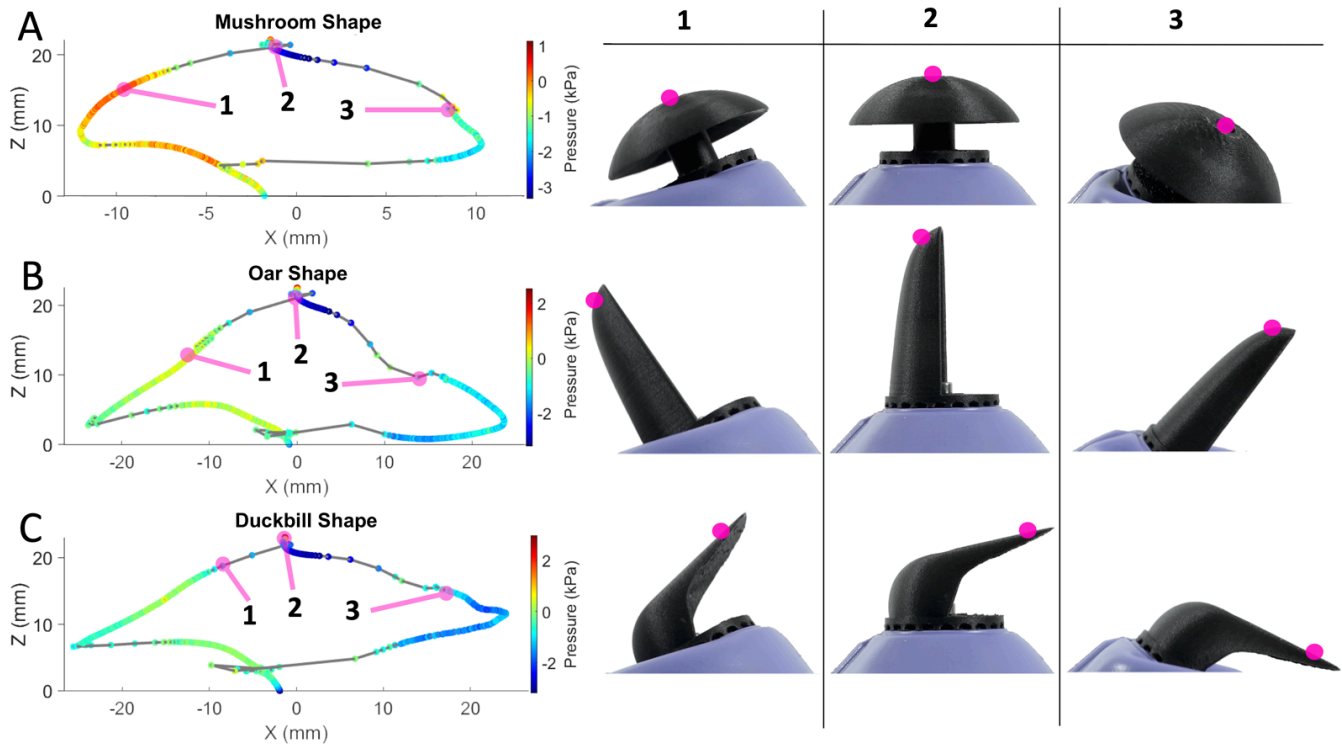


Fig. 9. Vicon tracking results for the actuation cycle of the three different end effectors. An infrared reflective tracker (denoted with a pink dot) was placed at the tip of each end effector to capture its full range of motion in an unloaded state. As expected, the inflation region of the stroke corresponded to higher pressures (left side of the graphs) and the deflation stroke corresponded to lower pressures (right side of the graphs).

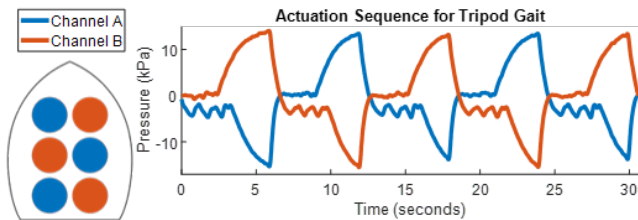


Fig. 10. Alternating actuation gait, where channel A (connecting three bi-stable domes) is phased  $180^\circ$  from channel B (connecting the other three bi-stable domes). The operating pressure ranges from 15 kPa to -15 kPa for each step/stroke, unloaded.

to produce the appropriate dome geometries, could also allow these actuators to precisely reproduce environmentally specific animal gaits in difficult to navigate habitats such as soft marine sediments. The incorporation of multiple hollow and individually inflatable ribs could also be used to modulate between in-plane and out of plane motion to create more complex 3D gaits. Downsizing the actuators for incorporation into large-scale arrays would also greatly increase their efficiency and usability, as is seen in sea stars, sea urchins, and other echinoderms. These animals contain thousands of small and simple actuators, all working in unison to create macroscopic displacements, and can navigate a wide range of challenging habitats by effectively reducing

single appendage substrate point loading to practically negligible quantities [18], [17], [29]. Having thousands of these simple actuators would be straightforward to manufacture through an injection molding or roll-to-roll process, and individual actuators could be damaged or disabled without detrimental consequences to the robot's performance in an open system.

On the system side, future work would involve developing a high efficiency pumping system that could pulse fluid rapidly to increase the gait cycle, or adapting existing work on a cyclic hydraulic pump by Katzschmann et al. to meet our pressure and volume requirements [19]. The current cycle frequency of 0.167 Hz was due to limitations in the pump's performance, which directly impacted the maximum speed of the robot. By using a hydraulic fluid, the pumping rate could be greatly increased if a pump similar to a reciprocating piston pump was employed, with the cycle rate only limited by the cavitation of the hydraulic fluid. Furthermore, the dome actuators would be able to handle a much higher payload as the fluid would be incompressible, thus making these actuators a viable option in the production of a diverse array of versatile soft robotic prototypes.

#### ACKNOWLEDGMENTS

The authors gratefully acknowledge support from the Office of Naval Research (award # N00014-17-1-

### References

- [1] K. L. Hoffman and R. J. Wood, "Towards a multi-segment ambulatory microrobot," in 2010 IEEE International Conference on Robotics and Automation, pp. 1196–1202, IEEE, 2010.
- [2] D. J. Hyun, J. Lee, S. Park, and S. Kim, "Implementation of trot-to-gallop transition and subsequent gallop on the MIT Cheetah I," *The International Journal of Robotics Research*, vol. 35, no. 13, pp. 1627–1650, 2016.
- [3] S. Kim, J. E. Clark, and M. R. Cutkosky, "ISprawl: Design and tuning for high-speed autonomous open-loop running," *International Journal of Robotics Research*, vol. 25, pp. 903–912, 9 2006.
- [4] Y. Yamada, Y. Miyagawa, R. Yokoto, and G. Endo, "Development of a Blade-type Crawler Mechanism for a Fast Deployment Task to Observe Eruptions on Mt. Mihara," *Journal of Field Robotics*, vol. 33, pp. 371–390, 5 2016.
- [5] B. Gorissen, D. Reynaerts, S. Konishi, K. Yoshida, J. W. Kim, and M. De Volder, "Elastic Inflatable Actuators for Soft Robotic Applications," *Advanced Materials*, vol. 29, 11 2017.
- [6] R. V. Martinez, A. C. Glavan, C. Keplinger, A. I. Oyetibo, and G. M. Whitesides, "Soft actuators and robots that are resistant to mechanical damage," *Advanced Functional Materials*, vol. 24, no. 20, pp. 3003–3010, 2014.
- [7] K. C. Galloway, K. P. Becker, B. Phillips, J. Kirby, S. Licht, D. Tchernov, R. J. Wood, and D. F. Gruber, "Soft Robotic Grippers for Biological Sampling on Deep Reefs," *Soft Robotics*, vol. 3, no. 1, pp. 23–33, 2016.
- [8] P. Boyraz, G. Runge, and A. Raatz, "An overview of novel actuators for soft robotics," *High-Throughput*, vol. 7, 9 2018.
- [9] A. D. Marchese, R. K. Katzschmann, and D. Rus, "A recipe for soft fluidic elastomer robots," *Soft Robotics*, vol. 2, pp. 7–25, 3 2015.
- [10] D. Rus and M. T. Tolley, "Design, fabrication and control of soft robots," *Nature*, vol. 521, no. 7553, p. 467–475, 2015.
- [11] A. D. Marchese and D. Rus, "Design, kinematics, and control of a soft spatial fluidic elastomer manipulator," *International Journal of Robotics Research*, vol. 35, pp. 840–869, 6 2016.
- [12] D. Drotman, M. Ishida, S. Jadhav, and M. T. Tolley, "Application-driven design of soft, 3-d printed, pneumatic actuators with bellows," *IEEE/ASME Transactions on Mechatronics*, vol. 24, pp. 78–87, 2 2019.
- [13] R. F. Shepherd, F. Ilievski, W. Choi, S. A. Morin, A. A. Stokes, A. D. Mazzeo, X. Chen, M. Wang, and G. M. Whitesides, "Multigait soft robot," *Proc. National Academy of Sciences*, vol. 108, no. 51, pp. 20400–20403, 2011.
- [14] D. Drotman, S. Jadhav, M. Karimi, P. de Zonia, and M. T. Tolley, "3d printed soft actuators for a legged robot capable of navigating unstructured terrain," in 2017 IEEE International Conference on Robotics and Automation (ICRA), pp. 5532–5538, May 2017.
- [15] S. Rozen-Levy, W. Messner, and B. A. Trimmer, "The design and development of branch bot: a branch-crawling, caterpillar-inspired, soft robot," *The International Journal of Robotics Research*, p. 0278364919846358, 2019.
- [16] N. W. Bartlett, K. P. Becker, and R. J. Wood, "A fluidic demultiplexer for controlling large arrays of soft actuators," *Soft Matter*, 2020.
- [17] B. Gorissen, M. de Volder, and D. Reynaerts, "Pneumatically-actuated artificial cilia array for biomimetic fluid propulsion," *Lab Chip*, vol. 15, pp. 4348–4355, 2015.
- [18] M. A. Bell, I. Pestovski, W. Scott, K. Kumar, M. K. Jawed, D. A. Paley, C. Majidi, J. C. Weaver, and R. J. Wood, "Echinoderm-inspired Tube Feet for Robust Robot Locomotion and Adhesion," *IEEE Robotics and Automation Letters*, vol. 3, pp. 2222–2228, 2018.
- [19] R. K. Katzschmann, A. D. Marchese, and D. Rus, "Hydraulic autonomous soft robotic fish for 3D swimming," in *Springer Tracts in Advanced Robotics*, vol. 109, pp. 405–420, Springer Verlag, 2016.
- [20] R. M. Neville, R. M. Groh, A. Pirrera, and M. Schenk, "Shape control for experimental continuation," *Physical review letters*, vol. 120, no. 25, p. 254101, 2018.
- [21] P. Rothmund, A. Ainla, L. Belding, D. Preston, S. Kurihara, Z. Suo, and G. M. Whitesides, "A soft, bistable valve for autonomous control of soft actuators," *Science Robotics*, vol. 3, pp. 1–10, 3 2018.
- [22] C. Balaguer, A. Gimenez, and A. Jardon, "Climbing Robots' Mobility for Inspection and Maintenance of 3D Complex Environments," *Autonomous Robots*, vol. 18, no. 2, pp. 157–169, 2005.
- [23] R. Hodoshima, S. Watanabe, Y. Nishiyama, A. Sakaki, Y. Ohura, and S. Kotosaka, "Development of asura i: Harvestman-like hexapod walking robot — approach for long-legged robot and leg mechanism design," in 2013 IEEE/RSJ International Conference on Intelligent Robots and Systems, pp. 4669–4674, Nov 2013.
- [24] J. Faigl and P. Čížek, "Adaptive locomotion control of hexapod walking robot for traversing rough terrains with position feedback only," *Robotics and Autonomous Systems*, vol. 116, pp. 136 – 147, 2019.
- [25] C. Li, T. Zhang, and D. I. Goldman, "A terradynamics of legged locomotion on granular media," *Science*, vol. 339, no. 6126, pp. 1408–1412, 2013.
- [26] X. Xiong, A. D. Ames, and D. I. Goldman, "A stability region criterion for flat-footed bipedal walking on deformable granular terrain," in 2017 IEEE/RSJ International Conference on Intelligent Robots and Systems (IROS), pp. 4552–4559, Sep. 2017.
- [27] Q. Pan and S. Guo, "Paddling type of microrobot in pipe," in 2009 IEEE International Conference on Robotics and Automation, pp. 2995–3000, May 2009.
- [28] Z. Driss, S. Karray, H. Kchaou, M. S. Abid, and M. S. Abid, "Computer simulations of fluid-structure interaction generated by a flat-blade paddle in a vessel tank," *International Review of Aerospace Engineering (IREASE)*, vol. 7, no. 3, 2014.
- [29] R. Santos, D. Haesaerts, M. Jangoux, and P. Flammang, "Comparative histological and immunohistochemical study of sea star tube feet (echinodermata, asteroidea)," *Journal of Morphology*, vol. 263, no. 3, pp. 259–269, 2005.